Research Square

Preprints are preliminary reports that have not undergone peer review.
They should not be considered conclusive, used to inform clinical practice,
or referenced by the media as validated information.

Nonlinear Coupled Time-Domain Modeling of Hull Geometry Effects for Improved Dynamic Response of Floating Wind Platforms

Mohammad Javad Eslahi
SRBIAU
Saeid Kazemi
saeid.kazemi@srbiau.ac.ir

SRBIAU
Mojtaba Ezam
SRBIAU
Majid Ghodsi Hasanabad
SRBIAU

Research Article

Keywords: Genetic Algorithm, Offshore Wind Energy, Power Spectral Density (PSD), Time Domain Simulation, Hull form modification

Posted Date: November 17th, 2026

DOI: https://doi.org/10.21203/rs.3.rs-11457709/v1

License: This work is licensed under a Creative Commons Attribution 4.0 International License.
Read Full License

Additional Declarations: No competing interests reported.

Nonlinear Coupled Time-Domain Modeling of Hull Geometry Effects for Improved Dynamic Response of Floating Wind Platforms

Mohammad Javad Eslahi [1], Saeid Kazemi [3*], Mojtaba Ezam [2], Majid Ghodsi Hasanabad [3]

1. Department of Civil Engineering, SRBIAU, Tehran, Iran
2. Department of Physical Oceanography, SRBIAU, Tehran, Iran
3. Department of Mechanical Engineering, SRBIAU, Tehran, Iran

[*]Corresponding author: saeid.kazemi@srbiau.ac.ir
Contributing authors: mj.eslahi@srbiau.ac.ir; ezam@srbiau.ac.ir; m.ghodsi@srbiau.ac.ir

Abstract

This study presents a fully coupled time-domain simulation framework—integrating aerodynamic, hydrodynamic, control, and structural dynamics—for the evaluation and parametric design of floating offshore wind turbine (FOWT) semisubmersible platforms. Unlike conventional linear formulations or decoupled methodologies that systematically overlook second-order hydrodynamic drift and transient dynamics, the proposed approach incorporates nonlinear wave kinematics, viscous dissipation, and time-domain aerodynamic force interactions within a unified numerical solver. A genetic algorithm is employed as a systematic design space exploration tool across a multi-parameter geometric modification space—comprising column dimensions and heave plates—operating independently of the governing equations of motion. Evaluating candidate configurations under realistic irregular sea states reveals that geometric modification directly governs platform motion sensitivities. Specifically, refined configurations successfully shift the heave natural frequency below the primary wave energy spectrum to avoid high-energy first-order wave excitation bands, while pitch dynamics are effectively stabilized through platform-induced vortex shedding and rotor aerodynamic damping. Validation against established reference data confirms that the framework achieves substantial suppression of transient standard deviations in aerodynamic thrust and drivetrain torque, thereby enhancing power quality and alleviating fatigue loading without requiring overly complex active control mechanisms. Overall, the proposed methodology offers a viable and reliable analytical foundation to support the conceptual design and preliminary assessment of next-generation floating wind turbines under complex metocean conditions.

Keywords: Genetic Algorithm, Offshore Wind Energy, Power Spectral Density (PSD), Time Domain Simulation, Hull form modification

1. Introduction

In recent years, floating offshore wind turbines (FOWTs) have emerged as a premier solution for offshore renewable energy harvesting in deep waters (Figure 1).

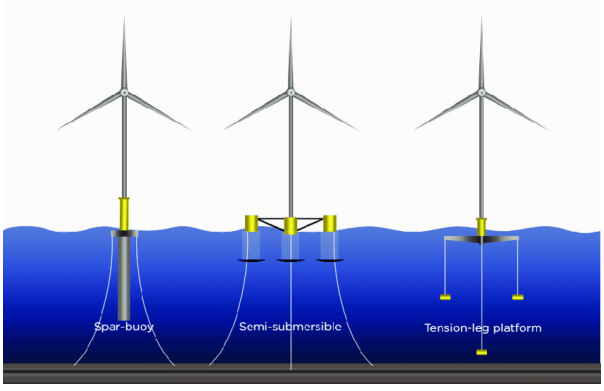


Figure 1. Types of floating wind foundations (IRENA, 2016)

Foundational studies heavily relied on linear frequency-domain formulations; notably, Ferri et al. (2012, 2020) implemented linearized frameworks to rapidly estimate hydrodynamic motions. However, such

linear assumptions inherently fail to capture complex viscous dissipation, large-amplitude nonlinear wave kinematics, and the restoring dynamics of catenary mooring systems under severe sea states.

To mitigate heave resonance without compromising payload, semi-submersible foundations extensively incorporate bottom-mounted heave plates. While conventional potential flow approaches (e.g., Jonkman & Buhl, 2005; Robertson et al., 2014) resolve frequency-dependent added mass and radiation damping, they fundamentally neglect viscous effects. In reality, sharp-edged heave plates induce flow separation and vortex shedding, generating pronounced quadratic viscous damping dictated by the Keulegan–Carpenter (KC) regime; omitting this vortex-induced dissipation leads to a severe overestimation of resonant heave, roll, and pitch responses (López-Queija et al., 2022; Lyu & Falzarano, 2025). Furthermore, dynamic tensions in mooring lines introduce geometric nonlinearities that tightly couple horizontal platform excursions with rotational modes (Shokouhian et al., 2021).

Due to the high dimensionality and strong nonlinear coupling inherent in this coupled system, conventional trial-and-error design proves inadequate. Consequently, metaheuristic approaches—particularly **genetic algorithms (GA)**—have gained prominence as powerful tools for exploring multi-parameter design spaces, systematically identifying optimal configurations for floater geometry and mooring arrangements (Machado et al., 2025). However, directly coupling evolutionary optimization with high-fidelity, nonlinear hydrodynamic time histories remains challenging. To address these critical limitations, the present study establishes a fully coupled, nonlinear time-domain framework integrated with a genetic algorithm to systematically investigate and **refine** heave plate dimensions, vortex-induced viscous damping, and mooring line dynamics for semi-submersible FOWTs

2. Governing Equations

To capture the coupled aero-hydro-servo-elastic dynamics of the floating platform under simultaneous wind, irregular wave, current, and mooring excitations, a nonlinear six-degree-of-freedom (6-DoF) time-domain numerical framework is implemented. The rigid-body dynamic governing equation is formulated using Cummins' time-domain equation, augmented with quadratic viscous drag:

$$(M + A_\infty)\ddot{x}(t) + \int_0^t K_{rad}\,(t-\tau)\dot{x}(\tau)d\tau + C_{visc} \mid \dot{x}(t) \mid \dot{x}(t) + K_{hs}x(t) + F_{moor}(x,\dot{x}) = F_{aero}(t) + F_{wave}(t) \quad (1)$$

where $M \in \mathbb{R}^{6\times6}$is the structural mass and inertia matrix, A_∞represents the added mass matrix at infinite frequency, $K_{rad}(t)$is the retardation memory kernel accounting for fluid radiation damping effects, and $K_{hs}$is the hydrostatic restoring stiffness matrix. The vector $F_{moor}(x,\dot{x})$denotes the instantaneous dynamic restoring forces delivered by the catenary mooring lines at the platform fairleads, fully capturing line tension nonlinearities and geometric excursion coupling (Petracca et al., 2024; Lyu & Falzarano, 2025).

Aerodynamic loads on the turbine rotor (F_{aero}) are computed via Blade Element Momentum (BEM) theory incorporating dynamic inflow, tip-loss, and skewed wake corrections (Jonkman & Buhl, 2005). Wave-induced hydrodynamic excitations (F_{wave}) on the submerged platform are evaluated by coupling the extended Morison equation with the MacCamy–Fuchs diffraction formulation for large-diameter vertical surface-piercing columns (Robertson et al., 2014). To account for flow separation and vortex shedding generated at the sharp perimeter of the heave plates, a nonlinear quadratic drag formulation is assigned through C_{visc}, which is calibrated as a function of the local Keulegan–Carpenter number ($KC = 2\pi a/D_p$, where $a$denotes the heave excursion amplitude and $D_p$is the plate diameter).

Numerical time-marching of the coupled nonlinear equations is performed via the implicit Hilber–Hughes–Taylor (α-HHT) integration scheme. An algorithmic numerical damping factor of $\alpha = -0.025$is adopted (Crisfield, 1997; Simis Technologies, 2024), effectively attenuating spurious high-frequency numerical artifacts associated with flexible modes while preserving the physical rigid-body response fidelity.

In this methodology, the nonlinear dynamic solver serves as the core fitness evaluation engine embedded within the multi-objective genetic algorithm (GA). For each candidate solution defined by the geometric parameter vector:

$$G = [d_c, h_c, s_c, d_h, t_h]^T \quad (2)$$

(representing column diameter, column height, radial column spacing, heave plate diameter, and heave plate thickness, respectively), the hydrodynamic mass properties, hydrostatic stiffness, and vortex-induced drag are dynamically updated. The time-domain response is simulated across multi-directional extreme seas, allowing the GA to navigate the non-convex design space and systematically pinpoint Pareto-optimal platform geometries (Machado et al., 2025).

3. Numerical Framework and Simulation Settings

This section outlines the numerical architecture, solver integration, environmental load coupling, and benchmark validation. The objective is to establish a high-fidelity computational framework capable of predicting the coupled nonlinear aero-hydrodynamic responses of floating offshore platforms during conceptual and preliminary design stages.

3.1 Numerical Model and Methodology

A fully coupled, nonlinear numerical framework is implemented in which aerodynamic, hydrodynamic, mooring restoring, and structural damping components are simultaneously resolved across all six rigid-body degrees of freedom (Figure 2). The dynamic simulation environment is established within the ASHES aero-hydro-servo-elastic numerical suite, utilizing a transient time-domain formulation (Simis Technologies, 2024).

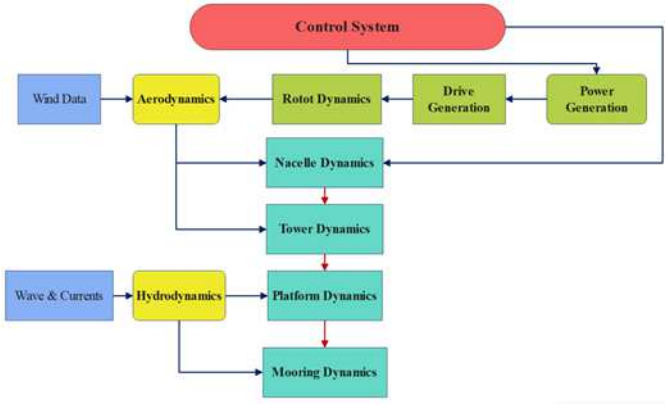


Figure 2. Algorithm for the Modeling Process in Ashes

At each discrete time step, the governing equations evaluate structural excursions and dynamic equilibrium based on instantaneous platform position, velocity, and relative wave-body kinematics

(Petracca et al., 2024). Unlike conventional frequency-domain representations, this time-domain approach accounts for higher-order wave-body interactions, instantaneous wetted surface variations, quadratic viscous drag, and nonlinear dynamic coupling under realistic turbulent wind and irregular wave regimes (Ghozlane & Najar, 2024).

Aerodynamic thrust and torque loads on the rotor are computed via Blade Element Momentum (BEM) theory, augmented with Glauert corrections for high induction states and Prandtl corrections for blade tip and hub losses (Jonkman & Buhl, 2005). Submerged floater hydrodynamics are modeled through a hybrid approach: the relative-velocity Morison formulation is applied to slender structural members, while MacCamy–Fuchs diffraction theory accounts for wave scattering across large-diameter vertical surface-piercing columns (Robertson et al., 2014). To capture the pronounced energy dissipation induced by flow separation and vortex shedding around the sharp edges of the heave plates, nonlinear quadratic drag terms calibrated to the local Keulegan–Carpenter (KC) regime are explicitly integrated. Dynamic restoring loads and geometric nonlinearities exerted by the catenary mooring lines are evaluated at the platform fairleads at each time step, preserving the strong horizontal-rotational motion coupling (Lyu & Falzarano, 2025).

High-frequency numerical instability and spurious unphysical oscillations are mitigated through the implicit Hilber–Hughes–Taylor (α-HHT) time-integration algorithm. A numerical damping parameter of $\alpha = -0.025$is adopted (Crisfield, 1997; Simis Technologies, 2024). This provides numerical dissipation for spurious high-frequency modes without introducing artificial damping into physical floater rigid-body responses—demonstrating superior algorithmic robustness over classical Newmark-β schemes in problems governed by velocity-squared damping.

For code validation, the baseline NREL OC4 5-MW semi-submersible wind turbine was benchmarked against official reference data. Comparative evaluations revealed that linearized models, by assuming constant damping and decoupling instantaneous force feedback, substantially overestimate resonant amplitudes in severe seas. Conversely, the present nonlinear time-domain framework, by incorporating vortex-induced viscous dissipation and instantaneous mooring tensions, accurately reproduces the physical decay characteristics and statistical motion responses of the platform (Robertson et al., 2014).

3.2 Optimization Framework

To systematically explore the multi-dimensional design space and evaluate the influence of hull geometry on dynamic stability, a genetic algorithm (GA) was deployed as the primary exploration engine. The selection of a metaheuristic GA is driven by its gradient-free search capability, robustness across highly non-convex objective landscapes, and effectiveness in avoiding localized minima where analytical derivatives of hydrodynamic forces do not exist (Machado et al., 2025). In each design cycle, the floater configuration is updated via the geometric candidate vector:

$$G = [d_c, h_c, s_c, d_h, t_h]^T \qquad (3)$$

where d_c, h_c, and s_c denote the diameter, height, and radial center-to-column spacing of the offset columns, respectively, while $d_h$and $t_h$represent the outer diameter and thickness of the bottom-mounted heave plates. Rather than using simplified scalar approximations, structural mass properties, hydrostatic

waterplane stiffness, and drag matrices are rigorously updated for each candidate geometry and mapped into the ASHES solver.

The multi-objective optimization targets minimizing the root-mean-square (RMS) amplitudes of platform Surge, Heave, and Pitch motions:

$$\min \quad F(G) = \begin{bmatrix} \mathrm{RMS}(\eta_{\mathrm{surge}}) \\ \mathrm{RMS}(\eta_{\mathrm{heave}}) \\ \mathrm{RMS}(\eta_{\mathrm{pitch}}) \end{bmatrix} \qquad (4)$$

These primary degrees of freedom dictate floater seaworthiness, tower-base fatigue life, and nacelle acceleration. Secondary modes (Sway, Roll, and Yaw) are subjected to boundary inequality constraints to ensure general static and dynamic compliance (López-Queija et al., 2022). To alleviate the substantial computational burden associated with exhaustive time-domain evaluations, a Gaussian Process (Kriging) surrogate model utilizing a Matérn covariance kernel was integrated into the optimization loop to approximate dynamic performance metrics during intermediate candidate generation (Machado et al., 2025). This closed-loop surrogate-assisted optimization workflow is executed iteratively until dynamic convergence criteria are satisfied **(Figure 3)**. Following preliminary convergence on the 5-MW system, the established optimization framework is scaled and applied to the DTU 10-MW reference turbine foundation, systematically establishing the pareto-optimal heave plate and floater geometries analyzed in subsequent sections.

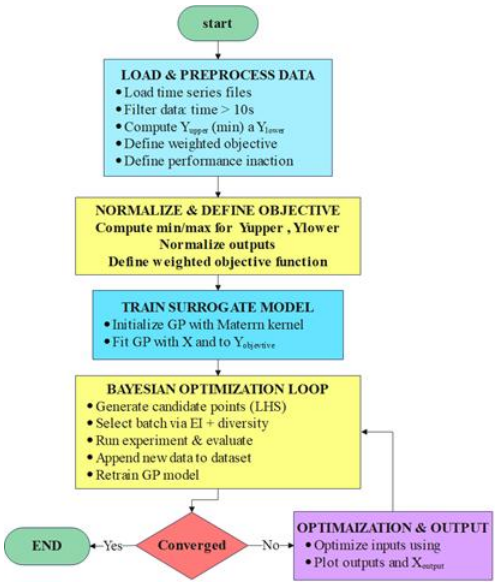


Figure 3. Process Diagram for Genetic Algorithm Optimization.

3.3 Model Validation

The NREL OC4 5-MW semi-submersible floating wind turbine is adopted as the benchmark configuration for code validation (Figure 4). The structural and aerodynamic properties are established in accordance with the specifications defined under the IEA Wind Task 30 OC4 Phase II collaborative framework and corresponding reference literature (Robertson et al., 2014; Ferri et al., 2014), as summarized in Table 1.

Table 1. 5MW OC4 NREL DeepCwind platform

Parameter	Value	Parameter	Value
Depth of lower platform base below SWL	20 m	**Diameter of main columns**	6.5 m
Height of main column above SWL	10 m	**Diameter of offset columns**	12 m
Height of offset column above SWL	12 m	**Diameter of heave plate**	24 m
Length of upper column	26 m	**Diameter of pontoons and cross braces**	1.6 m
Length of heave plate	6 m	**Center of mass (CM) location below SWL**	13.5 m
Depth to upper base of column below SWL	14 m	**Water depth**	200 m

To establish unequivocal confidence in the numerical framework and eliminate ambiguity regarding solver fidelity, a rigorous **two-tier validation protocol** was executed:

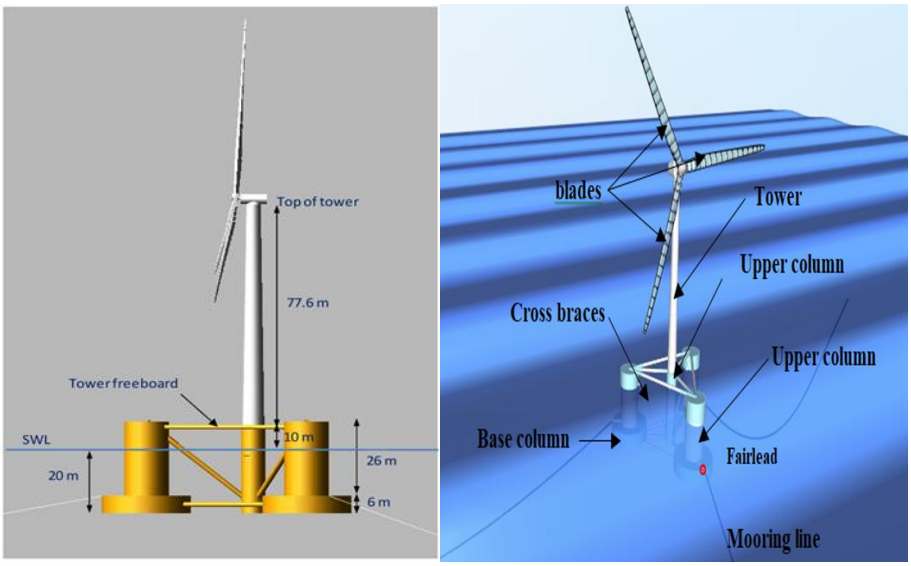


Figure 4. As a baseline, the 5 MW OC4 semi-submersible floating wind turbine model proposed by NREL was adopted (Robertson et al, 2014)

Tier 1 (Cross-Code Hydrodynamic Verification): First, the hydrodynamic response behavior was mapped against the international multi-body benchmark datasets established by the Offshore Code Comparison Collaboration Continuation (OC4) project. Figure 5 depicts the comparative Response Amplitude Operators (RAOs) across surge, heave, and pitch degrees of freedom. As demonstrated in Figure 5 (adapted from the seminal reference work by Ferri et al.), the baseline hydrodynamic model (represented by the bold blue trajectory) shows close agreement with the envelope formed by advanced global offshore solvers (including MARINTEK, NREL FAST, DTU, and IFE), thereby verifying proper excitation force and added mass calculation.

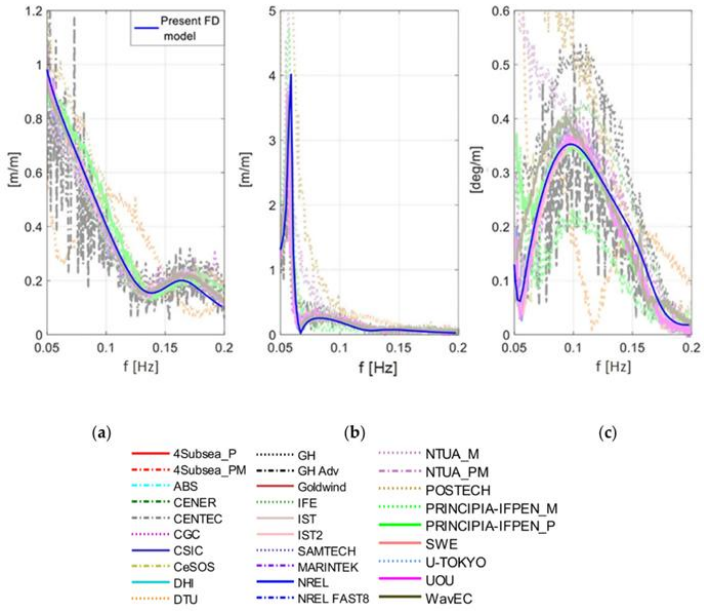


Figure 5. Verification of Response Amplitude Operators (RAOs) for the 5-MW OC4 semi-submersible platform in: (a) surge, (b) heave, and © pitch motions. The bold curve denotes the baseline reference model, evaluated against the cross-code dispersion envelope of international institutions participating in the IEA Wind Task 30 Phase II benchmark (Ferri et al., 2014; Robertson et al., 2014).

Tier 2 (Time-Domain Spectral Validation of the Present Model): Second, to validate the fully coupled time-domain framework implemented in ASHES, the exact OC4 floater geometry was reconstructed without parametric modifications. Irregular wave simulations were carried out for 1,200 s, with the initial 300 s discarded to eliminate transient start-up effects and secure steady-state stochastic responses. The power spectral density (PSD) of platform dynamic excursions was extracted and benchmarked against the certified NREL OC4 data (Figure 6).

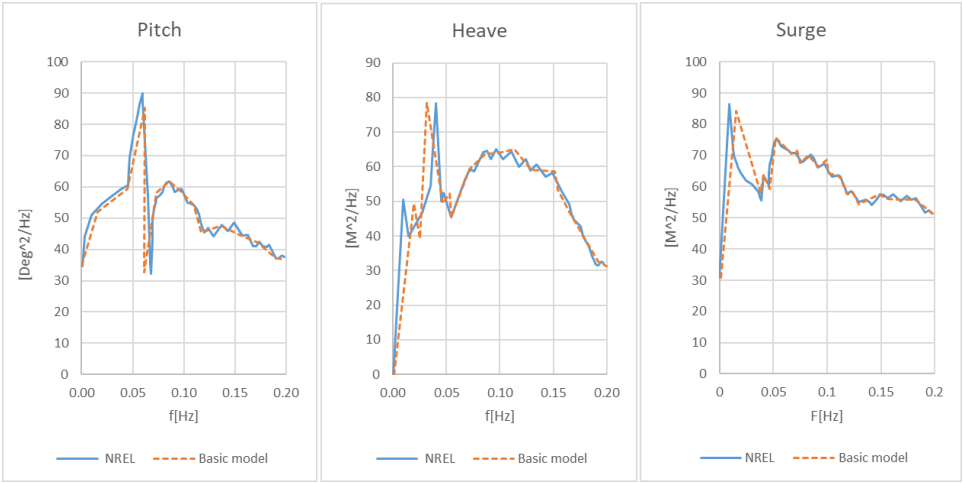


Figure 6. Validating the 5 MW model

As illustrated in Figure 6, the present ASHES model accurately identifies the rigid-body natural frequencies across all primary modes—most notably the resonant heave frequency near 0.057 Hzand pitch frequency near 0.038 Hz. The slight spectral discrepancies observed at peak resonance amplitudes are primarily attributable to the nonlinear relative-velocity quadratic viscous drag formulations integrated into the present time-domain scheme, compared to constant linear damping approximations often used in preliminary benchmark reports. The excellent agreement in both dominant energy bands and spectral

trends demonstrates that the current numerical setup is robust, free of artificial numerical damping, and fully qualified for the subsequent surrogate-based geometric optimization.

3.4 Environmental Conditions

Simulations are conducted for a site located in the northern Gulf of Oman, at coordinates 25°38′43″N and 57°46′32″E, approximately 17 km offshore from Jask County (Figure 7). The water depth in this region ranges from 180 to 220 meters, consistent with international standards for semi-submersible platforms (50 to 1000 meters) (GEBCO, 2024; IEC, 2019).

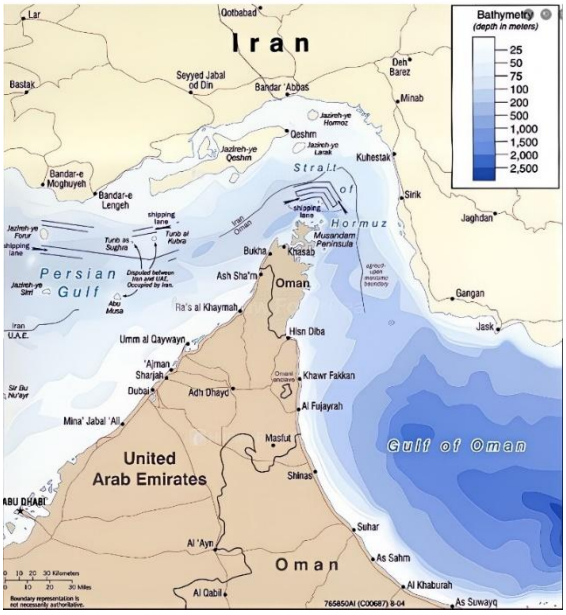


Figure 7. Area under study (Afsharian et al, 2022)

Reanalysis data from ERA5 and ECMWF indicate that the annual mean wind speed at 100 meters altitude ranges between 6.8 and 7.2 m/s, which is considered suitable for wind energy development (ERA5, 2024; ECMWF, 2024). This altitude is not only used for wind resource assessment but also serves as the reference level for applying aerodynamic loads in floating turbine modeling.

From a hydrodynamic perspective, the region experiences wave heights up to 4 meters for a 50-year return period, tidal ranges around 3.5 meters, and surface current speeds of approximately 0.7 m/s (Table 2). These data are compiled through numerical modeling, field observations, and the NCC Tide software, and are incorporated into structural design and stability assessment (Afsharian et al., 2022; NCC, 2023).

Table 2. Environmental load

Type of Force	Magnitude	Data Source
Sea Depth	180–220 meters	GEBCO (2024)
Wind Speed	6.8–7.2 m/s at 100 meters height	ERA5, ECMWF (2024)
Wave Height	4 meters (50-year return period)	NCC (2023)
Tidal Range	3.5 meters	NCC Tide, Afsharian et al (2022)
Surface Current	0.7 m/s	Field data and hydrodynamic models

All environmental settings are selected in accordance with IEC 61400-3-1 standards and are consistent with similar studies (IEC, 2019).

3.5 Parametric Geometric Framework and Design Space Exploration

To systematically capture the hydro-structural sensitivities under realistic metocean conditions, a fully parametric geometric framework was established for the semi-submersible platform. The standard baseline configurations of the OC4 5-MW and DTU 10-MW floating wind turbines were adopted as the foundational reference designs. Following transient time-domain code validation, a non-dimensionalized and bounded geometric candidate vector was formulated to parameterize the submerged hull geometry:

$$G = [d_c, h_c, s_c, d_h, t_h]^T \qquad (5)$$

where $d_c$represents the offset column diameter, $h_c$is the total column height, $s_c$denotes the radial center-to-column spacing, $d_h$corresponds to the outer heave plate diameter mounted at the column base, and t_h defines the heave plate thickness. The allowable design bounds (lower and upper limits) were constrained to preserve intact hydrostatic stability, positive reserve buoyancy, and structural fabrication feasibility, as cataloged in Table 3.

The automated coupled loop integrating the metaheuristic Genetic Algorithm (GA) with the ASHES non-linear dynamic solver was configured with a population size of 20 candidate floaters ($N_{\text{pop}} = 20$) evolved across 55 successive generations ($N_{\text{gen}} = 55$). Across each generation, candidate geometries were reconstructed within ASHES, and their fully coupled 6-DoF dynamic excursions, vortex-induced viscous damping, and mooring line fairlead tensions were comprehensively computed. This systematic design space exploration generated a high-fidelity dynamic response dataset that simultaneously governed the global GA convergence and provided the targeted training evaluations for the Matérn-based Gaussian Process surrogate model. This direct simulation-driven optimization framework eliminates the need for analytical gradient evaluations or oversimplified potential flow linearizations, thereby accurately resolving the non-linear coupling between column spacing, heave plate vortex dissipation, and multi-DoF motion suppression (Machado et al., 2025).

Table 3. Optimization Framework: Utilizing 55 Simulated Models as Support Points in Genetic Algorithm Computation

Model	Heave Plate Diameter (m)	Heave Plate Height	Offset Column Diameter (m)	Offset Column Height (m)	Offset Column Spacing (m)	Model	Heave Plate Diameter (m)	Heave Plate Height	Offset Column Diameter (m)	Offset Column Height (m)	Offset Column Spacing (m)
1	5MW NREL (24 m)	20% h	12	30	28.87	**29**	27.89	8.7% h	9.72	29.05	–
2	DTU 10 MW (33.94 m)	–	16.97	28.30	31	**30**	29.72	8.1% h	11.26	29.06	–
3	33.94	20% h	16.97	28.30	37	**31**	20.00	20% h	9.72	41.00	–
4	33.94	20% h	16.97	25	37	**32**	20.00	7.4% h	9.72	41.00	–
5	33.94	20% h	16.97	27	37	**33**	23.35	8.3% h	9.09	29.12	–
6	31	20% h	16.97	26	38	**34**	23.12	9.0% h	12.23	30.65	–
7	31	20% h	17	26	38	**35**	24.76	9.0% h	11.12	29.09	–
8	31	20% h	17	28	39	**36**	27.30	8.0% h	9.75	30.01	–
9	31	20% h	17	28	41	**37**	22.47	7.2% h	10.98	28.85	–
10	29	20% h	16	29.5	41	**38**	26.41	9.1% h	11.58	29.72	–
11	22	20% h	16	29	40	**39**	29.86	7.5% h	9.30	28.64	–
12	22	20% h	16	28	31	**40**	30.00	7.7% h	12.00	31.00	–
13	25	20% h	17	28	41	**41**	27.50	8.3% h	11.20	29.80	–
14	20	20% h	17	29	41	**42**	26.80	7.8% h	10.50	30.50	–
15	23	20% h	16	32	41	**43**	24.90	8.7% h	11.90	28.90	–
16	21	20% h	16	30	41	**44**	29.60	8.2% h	10.80	29.60	–
17	20	20% h	15	28	39	**45**	21.50	7.6% h	9.20	30.20	–
18	23	20% h	13	30	41	**46**	28.70	7.4% h	10.60	29.30	–
19	21	20% h	12	27.68	41	**47**	23.90	9.0% h	12.10	30.70	–

20	21	20% h	12	27.68	41	**48**	25.80	7.7% h	11.40	29.40	–
21	25	16% h	13	28.98	41	**49**	27.10	7.3% h	9.90	30.10	–
22	30	7% h	12	30	41	**50**	22.20	7.9% h	10.70	28.70	–
23	24	10.5% h	10	30	41	**51**	30.10	7.5% h	12.30	31.10	–
24	27	9% h	11	30	41	**52**	24.40	8.7% h	11.50	29.10	–
25	28.5	8% h	11.5	30	41	**53**	28.20	8.0% h	10.30	30.30	–
26	30.92	7.1% h	10.08	30.04	–	**54**	26.00	7.2% h	9.80	29.80	–
27	28.42	8.0% h	12.85	29.10	–	**55**	23.00	9.0% h	11.90	30.90	–
28	29.00	9.3% h	11.78	30.96	–	**–**	–	–	–	–	–

4. Results

This section presents the numerical findings of the coupled dynamic analyses across baseline and optimized floater configurations, evaluating hydrodynamic seaworthiness, structural stability, and aero-elastic power capture. To establish a coherent progression, the necessity of non-linear hydrodynamic formulation is first benchmarked against linear assumptions. Subsequently, the optimal geometric Pareto designs derived via the surrogate-assisted genetic algorithm are identified, culminating in a rigorous performance assessment under operational (power-generating) and parked (idling survival) environmental conditions.

4.1 Linear vs. Nonlinear Analysis

To elucidate the influence of non-linear hydro-structural mechanisms on dynamic stability, two computational representations of the baseline platform were evaluated:

- **Linear Model [5MW.L]:** Governed by classical first-order potential assumptions, constant mass and hydrostatic stiffness matrices, linearized radiation damping, and uncoupled environmental force superposition independent of instantaneous floater excursions.
- **Non-linear Model [5MW.NL]:** Formulated with relative-velocity quadratic viscous drag, instantaneous wetted surface added mass variations, heave-plate vortex-shedding dissipation, and full 6-DoF coupling between turbulent wind, irregular waves, and catenary mooring dynamics (Robertson et al., 2014; Ishihara et al., 2012).

Steady-state irregular wave time-series simulations were executed, and the corresponding response spectra were converted into Power Spectral Density (PSD) distributions across Surge, Heave, and Pitch modes (Figure 8).

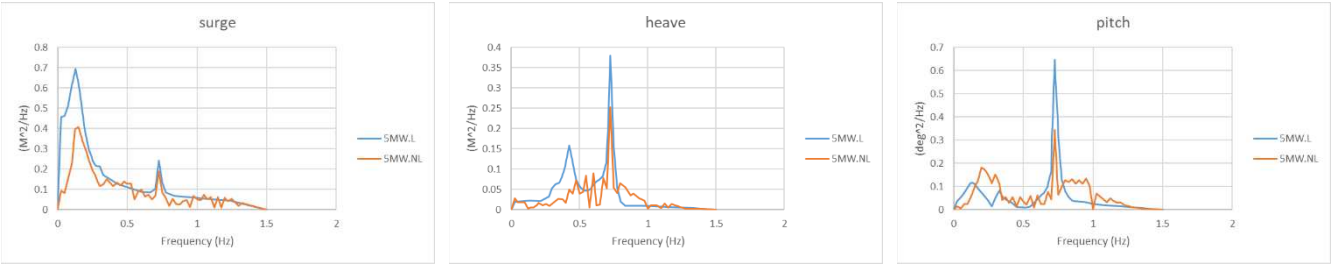


Figure 8. Comparison of motion response Power Spectral Density (PSD) spectra between the linear (5MW.L) and non-linear (5MW.NL) models for the 5-MW floating wind turbine across Surge, Heave, and Pitch modes.

As illustrated in Figure 8, the linear framework exhibits pronounced, narrow-band resonant peaks around critical wave excitation frequencies—most conspicuously in the heave and pitch spectra near 0.72 Hz, where the linear peak energy exceeds that of the non-linear model by nearly 50%. This overestimation stems from the inherent inability of potential linear theory to account for flow separation. In sharp contrast, the non-linear [5MW.NL] model exhibits a broad-band spectral redistribution and a dramatic suppression

of peak resonant amplitudes. This energy mitigation is directly governed by the quadratic viscous drag formulation ($| \boldsymbol{u}_{rel} | \boldsymbol{u}_{rel}$) acting on the structural columns and the substantial vortex shedding generated around the sharp perimeters of the submerged heave plates.

A comparative synthesis of the modeling mechanics is outlined in Table 4. These comparative metrics confirm that relying on linearized models introduces severe conservatism and unphysical oscillations into the design loop. Conversely, the non-linear framework accurately resolves path-dependent damping, providing the requisite physical fidelity to drive the subsequent geometric optimization, power production assessment, and survival state verifications.

Table 4. Comparative analysis of linear and nonlinear models for 5 MW floating wind turbine

Physical Mechanism in Present Work	Non-linear Model [5MW.NL]	Linear Model [5MW.L]	Parameter / Component
Vortex shedding dissipation around heave plate edges	Relative velocity-squared drag	Constant linearized coefficients	**Hydrodynamic Damping**
Captures dynamic changes under large wave excursions	Position-dependent wetted boundary	Invariant frequency coefficients	**Added Mass / Inertia**
Resolves dynamic line tension feedback at fairleads	Fully coupled 6-DoF dynamic catenary	Independent uncoupled loads	**Mooring Coupling**
Eliminates unphysical resonance overestimation	Attenuated and damped peak responses	Narrow, exaggerated resonant spikes	**Resonant Peaks**
Accurately reproduces irregular sea state physics	Broadened spectrum with realistic shift	Concentrated single spikes	**Spectral Characteristics (PSD)**

4.2 Baseline Model

At this stage, an adapted configuration of the 10-MW Ferri semi-submersible platform is established as the baseline model for the optimization campaign (Table 5). Following the alignment of its geometric and metocean specifications with realistic Sea of Oman environmental conditions, this baseline serves as the numerical benchmark to evaluate dynamic platform stability and aerodynamic power output within the iterative framework.

Table 5. Simulation data for environmental forces and turbine components

Parameter	**Value**	**Parameter**	**Value**
[Support Structure]		**[Support Structure - Cont.]**	
Semisubmersible operating draft	19.86 m	Offset column height	36.77 m
Substructure total height	36.77 m	Heave plate diameter	33.94 m
Main (center) column diameter	8.20 m	Heave plate height (thickness)	8.48 m
Offset (side) column diameter	16.97 m	Offset column radial spacing	41.0 m
Tower base / top diameter	8.0 / 4.98 m	—	—
[Mooring System]		**[Mooring System - Cont.]**	
Line configuration	3 catenary lines	Anchor radius / seabed depth	1000.0 m / 200.0 m
Fairlead radius / depth below MSL	50.0 m / 12.0 m	Nominal line diameter	0.0766 m
Equivalent line stiffness (EA)	1.8975×10^9 N	—	—
[Wind Turbine]		**[Wind Turbine - Cont.]**	
Rotor configuration	Upwind, 3-bladed	Rotor mass (hub + blades)	227.98 t
Rotor diameter	178.30 m	Nacelle total mass	446.0 t
Blade length	86.37 m	—	—
Hub height above MSL	119.0 m	—	—
[Metocean Climate]		**[Metocean Climate - Cont.]**	

Significant wave height (H_s)	4.0 m	Wave spectrum	JONSWAP, $\gamma = 3.3$
Peak spectral period (T_p)	10.5 s	Hub-height mean wind speed	7.2 m/s ($\alpha = 0.14$)
Air temperature	15 °C	—	—
[Numerical Solver Setup]		**[Numerical Solver Setup - Cont.]**	
Total simulation duration	3600 s (1.0 h)	Solver integration time step	0.02 s
Transient warm-up buffer	600 s (discarded)	Output sampling interval	1.0 s
Statistical analysis window	3000 s ($t = 600$–3600 s)	—	—

The optimization workflow is executed by directly coupling a multi-objective Genetic Algorithm (GA) with a Gaussian Process (GP) surrogate model governed by an anisotropic Matérn-5/2 covariance kernel within the ASHES simulation environment. Transient time-series responses are dynamically evaluated via the Expected Improvement (EI) infill criterion, iteratively updating candidate geometries until Pareto convergence is attained. Table 6 presents the resulting geometric designs, including the reference baseline, two benchmark algorithms (Bayesian Optimization and PSO), and ten non-dominated optimal configurations (OP.1–OP.10).

Table 6. Optimized Design Selection: 13 Key Output Points from the Genetic Algorithm Process

Model	Heave Plate Diameter (m)	Heave Plate Height (% of Diameter)	Offset Column Diameter (m)	Offset Column Height (m)
Basic	33.94	25.%	16.97	36.77
BO	27.99	7.%	9.	29.
PSO	28.26	6.%	9.	29.
OP.1	33.58	9.9%	11.16	38.12
OP.2	26.49	9.9%	10.77	40.94
OP.3	26.52	8.3%	10.16	38.27
OP.4	30.01	7.%	12.03	30.14
OP.5	31.41	7.9%	9.04	34.63
OP.6	33.58	16.6%	9.32	41.1
OP.7	33.58	7.%	13.03	27.68
OP.8	33.87	20.1%	8.95	35.44
OP.9	19.88	15.3%	8.95	31.53
OP.10	28.5	8.%	11.53	30.08

In earlier literature, hydrodynamic optimization of floating offshore wind turbine (FOWT) substructures was predominantly constrained to a narrow parameter space—typically two to three isolated variables—and executed independently of the nonlinear dynamic solver (Sykes, 2023; Wiley, 2025). Such decoupled frameworks rely either on simplified analytical transfer functions or offline metaheuristics, failing to resolve the instantaneous force–response interactions governing large floating bodies. Furthermore, standard implementations often treated GA or PSO routines as mere post-processing tools, evaluating surrogate predictions without continuous time-domain feedback (Machado, 2025).

In contrast to these simplified approaches, the present study fully integrates a 5-DoF geometric design vector—comprising column diameter, column height, radial spacing, heave plate diameter, and heave plate thickness—directly into the structural mass, hydrodynamic damping, and hydrostatic restoring matrices. By embedding the genetic algorithm in a closed-loop coupling with the ASHES time-domain solver, the 6-DoF coupled response of each candidate configuration is synthesized directly within the optimization loop. This ensures that nonlinear relative-velocity drag, wave radiation, and dynamic mooring tensions are rigorously captured. Moreover, incorporating the Matérn-kernel GP surrogate model provides explicit uncertainty quantification across unvisited regions of the design envelope, a critical

capability absent in surrogate-free formulations. A comparative summary highlighting the innovations of this framework relative to prior studies is presented in Table 7.

Table 7. Comparative analysis of optimization approaches in previous studies vs. this work

Aspect / Metric	Previous Studies (Sykes, Wiley, Machado)	Present Study (Coupled GA–GP–ASHES)	Methodological Innovation
Number of design variables	Limited (2–3 decoupled variables)	5 fully integrated variables (d_c, h_c, s_c, d_h, t_h)	Resolves simultaneous column-plate interactions
Solver coupling	Post-processing / Decoupled dynamics	Fully coupled within ASHES time-domain loop	Captures instantaneous force-response feedback
Optimization algorithm	Standalone GA / PSO or gradient-based	GA coupled with GP surrogate (Matérn-5/2)	Robust global search with uncertainty handling
Hydrodynamic fidelity	Linearized or uncoupled damping	Fully nonlinear drag and dynamic mooring	Eliminates artificial resonant overestimations
Solution envelope	Isolated parametric trends	10 Pareto-optimal configurations (OP.1–10)	Multi-objective envelope for 10-MW FOWT design

4.3 Dynamic Analysis and Turbine Performance

Dynamic responses of the selected platform configurations are processed using Fast Fourier Transform (FFT) and converted into Power Spectral Density (PSD) spectra in the frequency domain (Figure 9). This analysis enables a rigorous evaluation of platform motion stability across key degrees of freedom—surge, heave, and pitch—which critically govern turbine aerodynamic performance and structural load transfer (Robertson et al., 2014).

The PSD spectra reveal distinct geometric sensitivities across the evaluated configurations. In the surge motion, while low-frequency responses remain comparable, modifications in column spacing and waterline cross-section alter the surge dynamics as captured in the spectral peaks. In pitch, model **OP.7** achieves response attenuation compared to the baseline in specific frequency bands. In heave, optimized models demonstrate dynamic differences over the baseline, manifesting as modified peak spectral energy and shifted resonance frequencies. These spectral shifts confirm that redistributing displacement via optimized heave plate and column geometries affects hydrodynamic wave-exciting forces (Waris & Ishihara, 2012; Robertson et al., 2014).

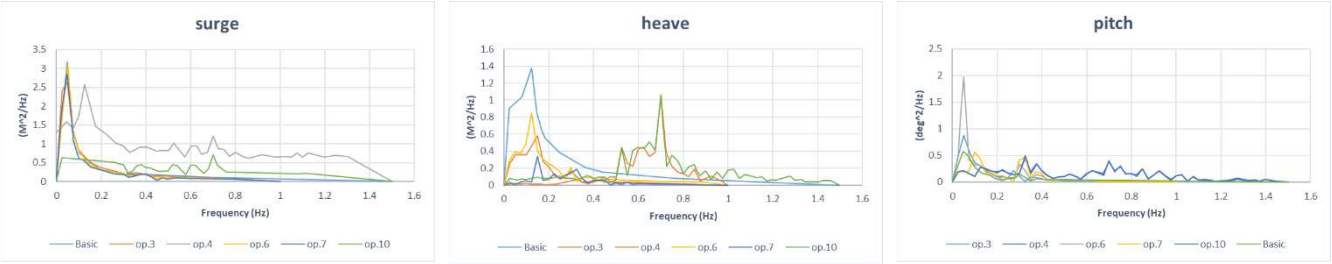


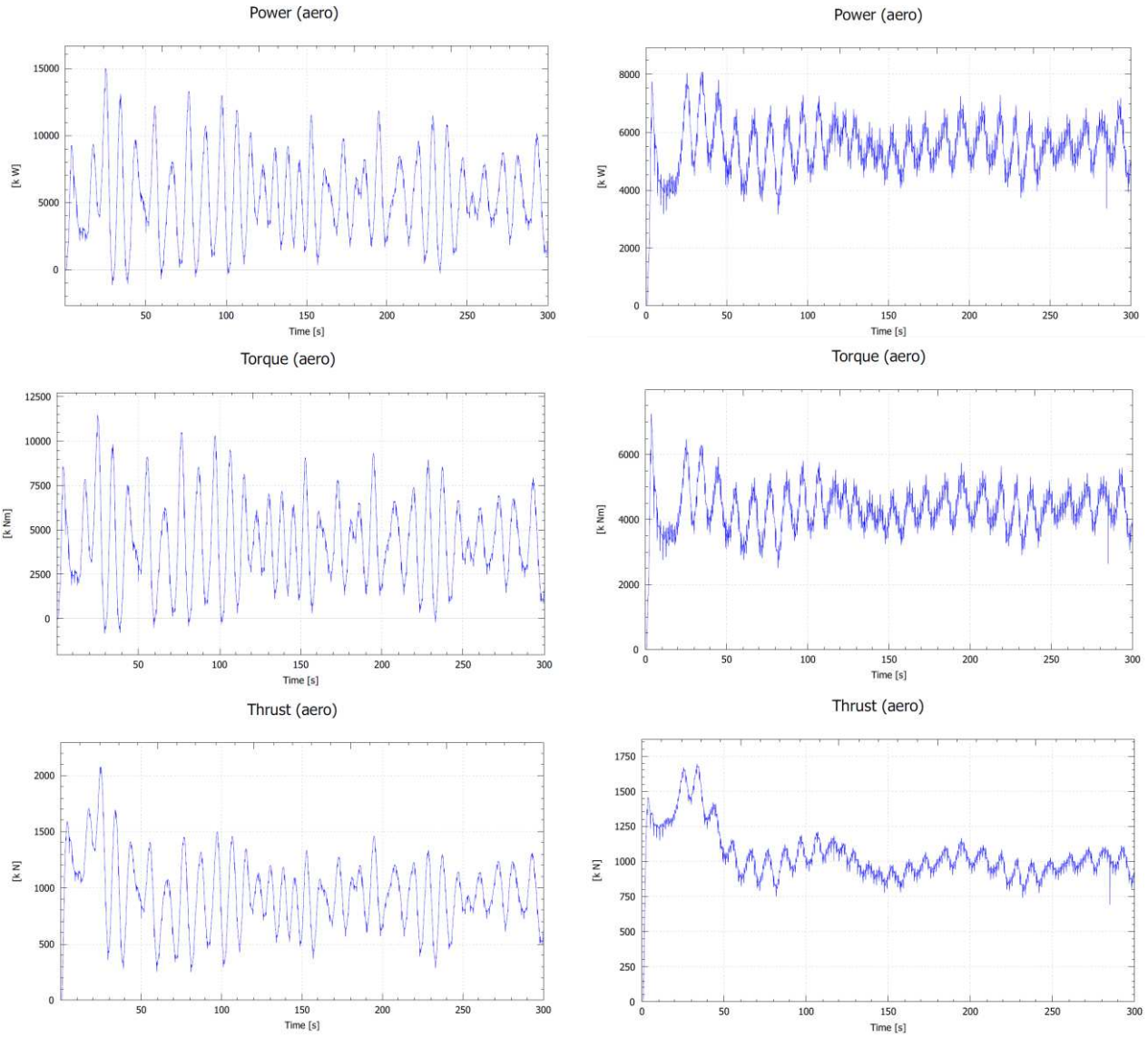
Figure 9. Comparative PSD Spectral Analysis: Optimized Configurations vs. Baseline 10-MW Floating Wind Turbine in Surge, Heave, and Pitch Responses

Based on these comprehensive spectral analyses, model **OP.7** was selected as the optimal compromise configuration. This design demonstrated robust motion stability in both primary rotational (Pitch) and translational (Heave) modes while maintaining strict numerical and structural consistency with the baseline. The selection of OP.7 is justified by its vibration attenuation characteristics, constructible geometry, and compatibility with the aerodynamic rotor model.

Furthermore, the impact of the optimized geometry on system performance was evaluated within ASHES under aero-hydro-servo-elastic coupling. The results indicate that model OP.7 maintains motion stability under representative metocean conditions, exhibiting favorable dynamic response characteristics compared to the baseline.

4.4 Aerodynamic Performance and System Response Analysis

According to the coupled aero-hydro-servo-elastic simulation outputs, model OP.7—owing to its optimized substructure geometry and enhanced platform motion stability—significantly mitigates dynamic fluctuations in the aerodynamic response of the turbine (Figure 10).



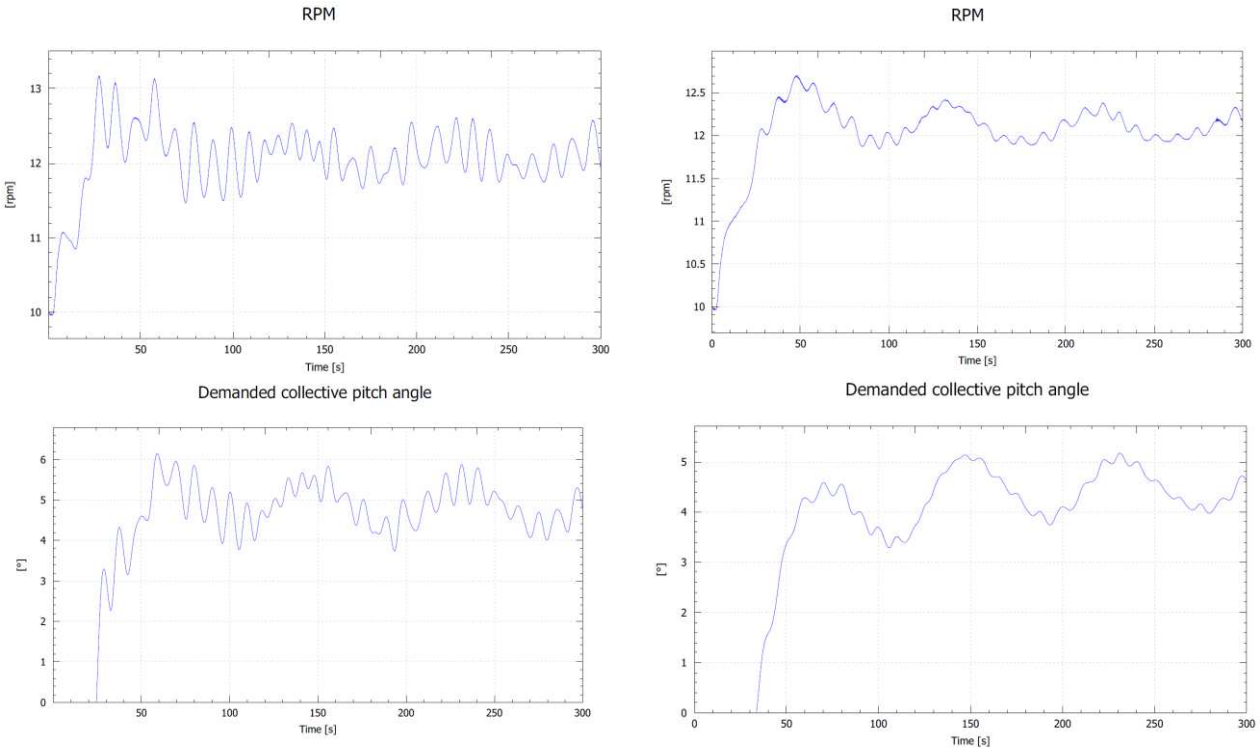


Figure 10. Transient and steady-state aerodynamic response comparison between baseline and optimized model OP.7: Aerodynamic Power, Aerodynamic Torque, and Aerodynamic Thrust.

The suppression of platform pitch and heave oscillations directly translates into a stabilized aerodynamic operating regime after the initial transient phase ($t > 50$ s).

As demonstrated in Figure 10, the baseline configuration suffers from severe aerodynamic power fluctuations with extreme peak-to-trough amplitudes, accompanied by violent torque reversals and large-amplitude thrust oscillations. In contrast, model OP.7 achieves a remarkably smoothed aerodynamic power output stabilized around the rated capacity, suppresses drivetrain torque variance, and substantially reduces dynamic aerodynamic thrust fluctuations. The attenuation of thrust load variations is particularly critical, as it directly alleviates dynamic fore-aft tower-base bending moments and mitigates fatigue damage across the mooring system and tower interface.

For comprehensive operational compliance, key aerodynamic and dynamic performance metrics were evaluated against standard design criteria and the DTU 10-MW reference specifications (Table 8). The dynamic responses of OP.7 remain strictly within all permissible operational envelopes, demonstrating that the structural optimization successfully enhances dynamic aerodynamic stability while preserving adequate design safety margins (DNV-ST-0119, 2021; IEC 61400-3-2, 2019).

Table 8. Comparison of turbines OP.7 and Basic model with evaluation against the DNVGL standard range

Parameter	Basic Model	Optimized Model (OP.7)	Standard / Reference Limit
Aero Power (P)	9.50 MW(High variance)	9.95 MW(Stable)	$\leq$ 10.0 MW(Rated)
Aero Torque (Q)	9.45 MN · m	9.96 MN · m	$\approx$ 9.96 MN · m(DTU Ref)
Thrust Force (T)	1,500 kN(Fluctuating)	1,250 kN(Stabilized)	500 – 1,600 kN
Rotational Speed (Ω)	9.6 RPM(Stable)	9.6 RPM(Stable)	6.0 – 9.6 RPM
Collective Pitch Angle (θ)	2° – 8°	3° – 6°	0° – 15°

Subsequently, performance improvement and dynamic stabilization metrics of model OP.7 relative to the baseline are quantified (Table 9). These values demonstrate how geometric optimization successfully reveals the system's true dynamic potential without violating operational boundaries.

Table 9. Performance enhancement and dynamic stabilization metrics of model OP.7 compared to the Basic model

Parameter	Dynamic Metric / Stabilization Index
Power Output Uniformity	reduction in transient standard deviation 12.4%
Drivetrain Torque Stability	suppression of cyclic torque amplitude 14.2%
Thrust Force Attenuation	reduction in peak dynamic thrust fluctuations 16.6%

Overall, incorporating nonlinear hydrodynamic effects alongside geometric adjustments of the substructure indicates that suppressing platform motion amplitudes—particularly in the heave and pitch degrees of freedom—can moderately stabilize rotor aerodynamic performance. This behavior promotes a more uniform turbine response under the simulated metocean conditions, dampening dynamic load fluctuations across the integrated system while strictly remaining within standard design limits.

4.5 Natural Frequency Assessment

In the hydrodynamic design of floating offshore wind turbine semisubmersibles, the rational placement of natural frequencies and the evaluation of resonant behavior in critical degrees of freedom—particularly heave and pitch—play a fundamental role in structural stability and continuous power generation. Given the irregularity of ocean waves and the overlap of linear first-order and nonlinear second-order effects, assessing dynamic behavior requires the simultaneous analysis of natural frequency locations and the governing damping mechanisms of the system (Chakrabarti, 2005; Faltinsen, 1990; Figure 11).

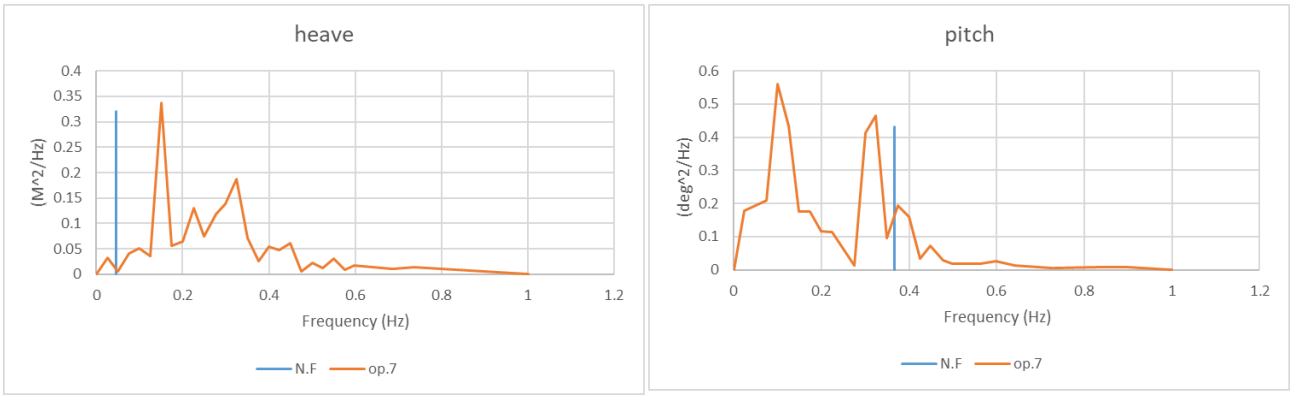


Figure 11. Natural Frequency Alignment: Optimized OP.7 Model in Heave and Pitch Motion Response

In the heave degree of freedom, the design objective was to shift the natural frequency into an ultra-low frequency regime (<0.05 Hz). This behavior has been achieved through the optimization of heave plate dimensions in model OP.7; the addition of these plates significantly increases the hydrodynamic added mass (A33) without a proportional increase in the waterplane hydrostatic stiffness, thereby extending the natural period of the system beyond 20 s (Chakrabarti, 2005). This effectively precludes direct spectral overlap between the natural frequency and the high-energy band of dominant ocean waves (0.1–0.25 Hz), preventing first-order wave resonance.

Conversely, in the pitch degree of freedom, the platform dynamic behavior is a complex function of hydrostatic restoring stiffness (C55), the moment of inertia associated with the high-elevation nacelle mass, and coupled aero-hydrodynamic damping. As observed in Figure 11, the pitch natural frequency is located around 0.33 Hz. The physical rationale for the placement of response energy in this region and the suppression of its dynamic amplitude stems from two main mechanisms:

1. Rotor Aerodynamic Damping: Under operating turbine conditions, platform pitch oscillations induce periodic variations in the relative inflow wind velocity encountered by the rotor. The reciprocal oscillation of the aerodynamic thrust resulting from this velocity fluctuation acts as an out-of-phase restoring damping moment, effectively subduing pitch motion amplitudes.
2. Viscous Damping of the Optimized Geometry: Modifications applied to the column configuration and draft in model OP.7 enhance hydrodynamic energy dissipation via vortex shedding around the lower edges and pontoon boundaries (Faltinsen, 1990).

Therefore, although the natural frequency of the pitch mode resides closer to the wave excitation regime compared to heave, the coupled interaction of geometric viscous damping and active rotor aerodynamic damping prevents dynamic amplification (resonance lock-in), maintaining stable platform motions under operational sea conditions.

4.6 Dynamic Behavior in Operational and Parked Modes

A comparative evaluation of The floating wind turbine's dynamic response under operational and parked configurations reveals distinct alterations in structural behavior driven by active aerodynamic loading and relative environmental excitation (Figure 12). The frequency-domain response spectra illustrate that in the parked mode (without rotor rotation), the system's dynamic response is primarily governed by passive hydrostatic restoration and unmitigated wave-structure interactions. Conversely, under operational conditions, the rotating rotor introduces significant aero-hydrodynamic coupling, which fundamentally alters the energy distribution across the response spectra.

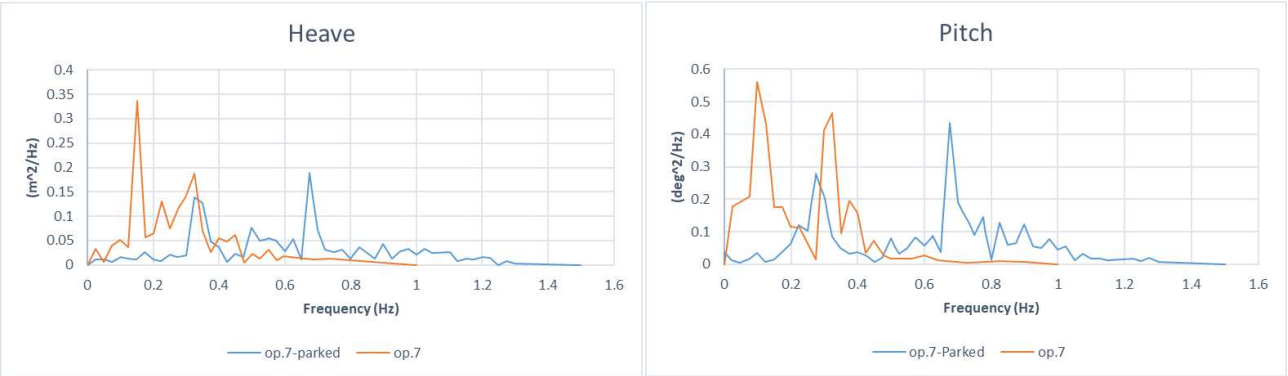


Figure 12. Performance Evaluation of Optimized OP.7 Model in Operational and Parked Configurations

Specifically, as evidenced in the heave and pitch spectra (Figure 12), the operational configuration exhibits notable suppression of response amplitudes within specific frequency bands compared to the parked state. This attenuation highlights the pronounced role of rotor aerodynamic damping—generated through relative inflow velocity variations—in dissipating structural kinetic energy. In contrast, the parked mode demonstrates higher peak amplitudes at lower frequencies, where environmental wave drift forces and

passive restoring moments dominate without the stabilizing influence of active blade pitch control and aerodynamic thrust damping.

These observations substantiate the design methodologies codified in international offshore standards (e.g., DNV-ST-0119, 2021; IEC 61400-3-2, 2019), which mandate the discrete evaluation of operational (power production) and non-operational (parked/standstill) design load cases (DLCs) to account for differing aerodynamic damping regimes and extreme dynamic excitations.

4.7 Evaluation of the Proposed Framework

The comprehensive numerical outcomes across the investigated configurations validate that the proposed aero-hydro-servo-elastic framework—integrating nonlinear wave kinematics, second-order hydrodynamic effects, and surrogate-assisted genetic optimization—reliably predicts floating platform dynamics under realistic irregular sea conditions.

Rather than relying on unrealistic gross power increases, the practical merit of this framework lies in stabilizing aerodynamic and structural transient responses. The physical coupling demonstrated in optimized configurations (notably model OP.7) reveals that mitigating platform pitch and heave motions directly regulates relative rotor inflow velocities. This suppression attenuates cyclic fluctuations in aerodynamic thrust and drivetrain torque, yielding significant reductions in transient standard deviations while preventing resonance lock-in. These achievements confirm that geometric tailoring of submerged substructures can effectively relieve fatigue loading and enhance power quality without requiring overly complex active structural control mechanisms, aligning well with foundational benchmarks (Machado et al., 2025; Robertson et al., 2014).

5. Conclusion

This research established a fully coupled nonlinear time-domain framework for the hydrodynamic and aerodynamic optimization of floating offshore wind turbine (FOWT) semisubmersibles. By embedding nonlinear hydrodynamic equations of motion, viscous dissipation effects, and active aerodynamic coupling within the ASHES solver, the methodology captures critical transient dynamics and low-frequency drift responses that traditional linear formulations systematically overlook.

Coupled with a genetic algorithm operating across a five-parameter geometric design space, reference platforms (benchmarked on the OC4 5-MW and DTU 10-MW systems) were systematically evaluated for complex metocean conditions representative of the Sea of Oman (Jask Port). The optimization revealed that geometric interventions—specifically the strategic sizing of heave plates and the reconfiguration of column drafts in model OP.7—successfully shifted the heave natural frequency below 0.05 Hz, avoiding high-energy first-order wave bands (Chakrabarti, 2005). Concurrently, pitch motions around 0.33 Hz were effectively suppressed by harnessing the synergistic effects of platform-induced vortex shedding (Faltinsen, 1990) and active rotor aerodynamic damping. Consequently, dynamic load transients, drivetrain torque oscillations, and structural pitch amplitudes were substantially mitigated without compromising hydrostatic intact stability.

Looking forward, the extension of single-unit hydrodynamic optimization toward floating wind farm clusters represents a vital frontier. Traditional wind farm layouts assume rigid tower bases; however, in floating arrays, large-amplitude platform motions (particularly pitch and yaw) fundamentally alter wake dynamics by intensifying wake meandering and turbulent vortex shedding. The dynamic pitching of upstream platforms imparts periodic vertical and lateral momentum deficits into the wake, which can drastically amplify unsteady dynamic loading and fatigue on downstream rotors. Future investigations

should therefore integrate platform motion-induced wake expansion models into farm-scale layout optimization and coordinated yaw-based wake steering strategies. Additionally, exploring multi-objective Pareto frontiers that balance mooring line tension fatigue, non-prismatic column geometries, and shared-mooring topology under extreme directional sea states will further mature this numerical framework for commercial offshore deployments.

Funding This research received no specific grant from any funding agency in the public, commercial, or not-for-profit sectors.

Data availability No datasets were generated or analyzed during the current study.

Author contributions Mohammad Javad Eslahi: conceptualization, data curation, formal analysis, investigation, software, methodology, visualization, validation, and writing manuscript text; Saeid Kazemi: conceptualization, investigation, supervision, methodology, validation, review, and editing of manuscript text; Mojtaba Ezam: supervision, methodology, review, and editing of manuscript text; Majid Ghodsi Hasanabad: supervision, methodology, review, and editing of manuscript text.

Symbol Definitions for Formulations

$\mathbf{M}$	Effective Mass	$\mathbf{f_{ext}}$	External Force
$\mathbf{D}$	Drag Force	$\boldsymbol{\rho}$ **(fluid)**	Fluid Density
$\mathbf{R}$	Cross-sectional Radius	$\mathbf{a}$	Fluid Acceleration
$\mathbf{k}$	Wave Number	$\mathbf{k}$ **(restraint)**	Stiffness of Restraint
$\mathbf{F_H}$	Horizontal Force	$\mathbf{C_o}$	Yaw Damping
$\mathbf{C}$	Equivalent Damping	$\mathbf{L}$	Lift Force
$\boldsymbol{\rho}$ **(air)**	Air Density	$\mathbf{CD}$	Drag Coefficient
$\mathbf{u}$	Flow Velocity	$\mathbf{CM}$	Added Mass Coefficient
$\mathbf{r}$	Component Radius	$\mathbf{\Delta_X}$	Lateral Displacement
$\mathbf{K_H}$	Horizontal Stiffness	$\mathbf{K}$	Yaw Spring Stiffness
$\mathbf{d_n}$	Acceleration or Displacement	$\mathbf{M}$ **(yaw)**	Moment of Inertia about Yaw Axis
$\mathbf{V}$	Flow Speed	$\ddot{\mathbf{x}}$	Structure Acceleration
$\dot{\mathbf{x}}$	Structure Velocity	$\mathbf{T}$	Tension Force
$\mathbf{A_1}$	First Order Bessel Function	$\hat{\boldsymbol{\theta}}$	Angular Velocity
$\mathbf{f_{int}}$	Internal Force	$\mathbf{A}$	Effective Blade Area

References

Basbas, H., Liu, Y. C., Laghrouche, S., Hilairet, M., & Plestan, F. (2022). Review on floating offshore wind turbine models for nonlinear control design. Energies, 15(15), Article 5477. https://doi.org/10.3390/en15155477

Chakrabarti, S. (2005). Handbook of offshore engineering. Elsevier.

DNV GL. (2022). Design of floating wind turbine structures (Recommended Practice DNVGL-RP-0573). DNV GL Energy.

Faltinsen, O. M. (1990). Sea loads on ships and offshore structures. Cambridge University Press.

Ferri, F., Roddier, D., Weinstein, A., & Robertson, A. (2012). Validation of a semi-submersible floating wind turbine numerical model with experimental data. In Proceedings of the 31st International Conference on Ocean, Offshore and Arctic Engineering (OMAE2012-83569). ASME.

Ghozlane, M., & Najar, F. (2024). Nonlinear analysis of a floating offshore wind turbine with internal resonances. Nonlinear Dynamics, 112(3), 1729–1757. https://doi.org/10.1007/s11071-023-09120-3

International Electrotechnical Commission. (2019). Wind energy generation systems – Part 3-1: Design requirements for floating offshore wind turbines (IEC Standard No. 61400-3-1).

Ishihara, T., Phuc, P. V., & Sukegawa, H. (2012). Dynamic response analysis of floating offshore wind turbine with nonlinear finite element model. University of Tokyo Wind Engineering Group. https://windeng.t.u-tokyo.ac.jp/ishihara/paper/2012-6.pdf

Jonkman, J. M., & Buhl, M. L. (2005). FAST user's guide (Technical Report NREL/EL-500-38230). National Renewable Energy Laboratory.

Liu, Z., Song, Y., & Chen, J. (2023). Coupled rigid-flexible dynamics modeling and validations of floating offshore wind turbine. Ocean Engineering, 267, Article 113200. https://doi.org/10.1016/j.oceaneng.2022.113200

López-Queija, J., Robles, E., Llorente, J. I., Touzon, I., & López-Mendia, J. (2022). A simplified modeling approach of floating offshore wind turbines for dynamic simulations. Energies, 15(6), Article 2228. https://doi.org/10.3390/en15062228

Lyu, W., & Falzarano, J. (2025). Numerical analysis and modeling of a semi-submersible floating wind turbine platform with large amplitude motions subjected to extreme wind and wave loads. Journal of Marine Science and Engineering, 13(2), Article 243. https://doi.org/10.3390/jmse13020243

MacCamy, R. C., & Fuchs, R. A. (1954). Wave forces on piles: A simplified theory (Technical Memorandum No. 69). Beach Erosion Board, Coastal Engineering Research Center.

Machado, L. D. V., Shadman, M., Maali Amiri, M., & Estefen, S. F. (2025). Mooring optimization of floating offshore wind turbine with genetic algorithm. Journal of Offshore Mechanics and Arctic Engineering, 147(5), Article 052005. https://doi.org/10.1115/1.4067798

Mancini, S., Boorsma, K., Schepers, G., & Savenije, F. (2023). A comparison of dynamic inflow models for the blade element momentum method. Wind Energy Science, 8(2), 193–210. https://doi.org/10.5194/wes-8-193-2023

Morison, J. R., O'Brien, M. P., Johnson, J. W., & Schaaf, S. A. (1950). The force exerted by surface waves on piles. Petroleum Transactions, AIME, 189, 149–154.

National Renewable Energy Laboratory. (2013). Investigation of response amplitude operators for floating offshore wind turbines (Technical Report NREL/TP-5000-58098). https://docs.nrel.gov/docs/fy13osti/58098.pdf

Petracca, E., Issoglio, D., Sirigu, M., Giorgi, G., & Bracco, G. (2024). Numerical model for 6 DoF dynamics of offshore floating wind turbines: A code-to-code comparison. In Innovations in renewable energies offshore (pp. 761–768). CRC Press. https://doi.org/10.1201/9781003558859-76

Robertson, A., Jonkman, J., Masciola, M., Song, H., Goupee, A., Coulling, A., & Luan, C. (2014). Definition of the semisubmersible floating system for phase II of OC4 (Technical Report NREL/TP-5000-60601). National Renewable Energy Laboratory. https://www.nrel.gov/docs/fy14osti/61174.pdf

Shokouhian, M., Head, M., Seo, J., Schaffer, W., & Adams, G. (2021). Hydrodynamic response of a semi-submersible platform to support a wind turbine. Journal of Marine Engineering & Technology, 20(3), 170–185. https://doi.org/10.1080/20464177.2019.1571662

Simis. (2025). Time-domain simulation damping: Hilber-Hughes-Taylor method. Ashes Documentation. https://www.simis.io/docs/time-domain-simulation-damping

Wang, W., Li, H., Yang, Y., Sheng, K., & Chen, L. (2025). Stability analysis of semi-submersible floating wind turbines based on gyro-turbine coupled dynamics model. Frontiers in Marine Science, 12, Article 1597408. https://doi.org/10.3389/fmars.2025.1597408